






Article

An SPS-RS Technique for the Fabrication of SrMoO₄ Powellite Mineral-like Ceramics for ⁹⁰Sr Immobilization

Anton A. Belov ¹, Oleg O. Shichalin ^{1,*}, Evgeniy K. Papynov ¹, Igor Yu. Buravlev ¹, Arseniy S. Portnyagin ¹, Semen A. Azon ¹, Alexander N. Fedorets ¹, Anastasia A. Vornovskikh ¹, Erhan S. Kolodeznikov ¹, Ekaterina A. Gridasova ¹, Anton Pogodaev ¹, Nikolay B. Kondrikov ¹, Yun Shi ^{2,3,*} and Ivan G. Tananaev ^{1,4}

¹ Nuclear Technology Laboratory, Department of Nuclear Technology, Institute of High Technologies and Advanced Materials, Far Eastern Federal University, 10 Ajax Bay, Russky Island, 690922 Vladivostok, Russia; papynov@mail.ru (E.K.P.); buravlev.i@gmail.com (I.Y.B.); arsuha@gmail.com (A.S.P.); azon.sa@dvfu.ru (S.A.A.); fedorets.alexander@gmail.com (A.N.F.); vornovskikh_aa@dvfu.ru (A.A.V.); pogodaev.av@dvfu.ru (A.P.); kondrikov.nb@dvfu.ru (N.B.K.)

² Shanghai Institute of Ceramics, Chinese Academy of Sciences, Shanghai 201899, China

³ Center of Materials Science and Optoelectronics Engineering, University of Chinese Academy of Sciences, Beijing 100049, China

⁴ Tananaev Institute of Chemistry and Technology of Rare Elements and Mineral Raw Materials, Kola Science Center, Russian Academy of Sciences, Akademgorodok, 26a, 184209 Apatity, Russia

* Correspondence: oleg_shich@mail.ru (O.O.S.); shiyun@mail.sic.ac.cn (Y.S.)

Abstract: This paper reports a method for the fabrication of mineral-like SrMoO₄ ceramics with a powellite structure, which is promising for the immobilization of the high-energy ⁹⁰Sr radioisotope. The reported method is based on the solid-phase “in situ” interaction between SrO and MoO₃ oxides initiated under spark plasma sintering (SPS) conditions. Dilatometry, XRD, SEM, and EDX methods were used to investigate the consolidation dynamics, phase formation, and structural changes in the reactive powder blend and sintered ceramics. The temperature conditions for SrMoO₄ formation under SPS were determined, yielding ceramics with a relative density of 84.0–96.3%, Vickers microhardness of 157–295 HV, and compressive strength of 54–331 MPa. Ceramic samples demonstrate a low Sr leaching rate of 10⁻⁶ g/cm²·day, indicating a rather high hydrolytic stability and meeting the requirements of GOST R 50926-96 imposed on solid radioactive wastes. The results presented here show a wide range of prospects for the application of ceramic matrixes with the mineral-like composition studied here to radioactive waste processing and radioisotope manufacturing.

Keywords: ceramics; strontium molybdate; powellite; radionuclides; radioactive waste management; solid-phase synthesis; SPS



Citation: Belov, A.A.; Shichalin, O.O.; Papynov, E.K.; Buravlev, I.Y.; Portnyagin, A.S.; Azon, S.A.; Fedorets, A.N.; Vornovskikh, A.A.; Kolodeznikov, E.S.; Gridasova, E.A.; et al. An SPS-RS Technique for the Fabrication of SrMoO₄ Powellite Mineral-like Ceramics for ⁹⁰Sr Immobilization. *Materials* **2023**, *16*, 5838. <https://doi.org/10.3390/ma16175838>

Academic Editors: Lidija Čurković and Changchun Ge

Received: 12 July 2023

Revised: 4 August 2023

Accepted: 22 August 2023

Published: 25 August 2023



Copyright: © 2023 by the authors. Licensee MDPI, Basel, Switzerland. This article is an open access article distributed under the terms and conditions of the Creative Commons Attribution (CC BY) license (<https://creativecommons.org/licenses/by/4.0/>).

1. Introduction

Mineral-like ceramics based on alkali-earth tungstates [1], molybdates [2–4], niobates [5], vanadates [6,7], etc., are actively studied as promising materials for the immobilization of radioactive wastes (RAW) in the form of solid matrixes for long-term storage. One of the best examples of these is the molybdate of a powellite structure that naturally occurs as CaMoO₄, adopting a scheelite-type tetragonal phase (space group I 4 1/a, Z = 4). Molybdates are of particular interest due to their outstanding luminescence properties, which are applied in gas detectors [8,9], optical devices [10–15], and scintillation detectors [16–19]. Different synthesis and processing techniques lead to changes in structural properties, which affect the material properties and comprise a motivating factor in the investigation of the formation of SrMoO₄. The interest in the field of immobilization comes from the structural variability that is due to the ability of molybdenum to reach several oxidation states (Mo⁶⁺, Mo⁵⁺, Mo⁴⁺, Mo³⁺); however, under oxidizing or neutral

conditions, most molybdenum ions are hexavalent, existing as $[\text{MoO}_4]_2$ -tetrahedra [20]. The structural flexibility of powellite allows the substance to tolerate large chemical substitutions including actinoid and lanthanide elements [2]. For example, Ca^{2+} cations in this structure can be partially or completely replaced with Sr^{2+} , Ba^{2+} , Cu^{2+} , Mn^{2+} , Cd^{2+} , Pb^{2+} , Cr^{2+} , and Fe^{2+} , and with rare-earth elements $\text{Nb}^{+2/+4}$, Ta^{+5} , and W^{+6} [20]. In other words, isostructural molybdate-like compounds can contain numerous elements, the isotopes of which are found in RAW [21]. Furthermore, Mo introduction into multicomponent highly active RAW at the level of 10 wt.% promotes the formation of the crystalline powellite phase, which has a positive effect on phase stability of the compound, as was previously shown based on the stability improvement in glasses [22].

Out of a large number of radionuclides that have to be immobilized, ^{90}Sr is of particular importance. This radionuclide is characterized by high specific activity, a long half-life period, and the ability to activate heat generation. ^{90}Sr is derived via β decay of ^{90}Rb and its isotopes, followed by a similar decay pathway into ^{90}Y . The latter one is also radioactive, with a half-life period of 64 h and β decays into ^{90}Zr . In this respect, the choice of the matrix for ^{90}Sr immobilization also accounts for the high liberated energy of the radioactive β decay of strontium itself (545.9 MeV) and its ^{90}Y derivative (~2.28 MeV), which can irreversibly affect the physicochemical nature of the materials. Apart from that, strontium's features, such as the ability to self-heat, gas migration, and high mobility in liquid media, are also put into consideration.

Several techniques are used to synthesize SrMoO_4 , including the Czochralski method [13], coprecipitation [7,18], traditional solid-phase reactions [12,23], sol-gel synthesis [9], hydrothermal synthesis [17], and microwave hydrothermal synthesis [15,16].

Among modern methods for the fabrication of RAW-immobilizing ceramics, one should pay special attention to spark plasma sintering (SPS) technology. The main principle is based on the rapid heating of the powder material in a vacuum by passing pulses of direct current through the graphite die with the sample while applying uniaxial pressure. SPS is characterized by a high heating rate, which allows us to shorten the fabrication time, reduce the cost of manufacturing, and improve the quality in comparison with the known counterparts. [24]. Successful examples of SPS application for solid-state matrix fabrication to immobilize RAW, including the ones with Sr, are in reports on studies of ceramics with structures of NZP, sinroc, garnet, whitlockite, perovskite, and others [25–27]. Additionally, the application of SPS technology was first implemented for the fabrication of radioisotope prototypes in the form of ionizing irradiation sources based on ceramic cores as active zones [28], some of which contain Sr [26,29].

In addition to that, a number of studies demonstrated high prospects for the implementation of SPS coupled with reactive sintering (SPS-RS) [30]. This approach is based on the “in situ” interaction between the components of the starting powder blend leading to the formation of ceramics composition different from that of reagents. Solid-state reaction between reagents is initiated under SPS conditions below their melting points [31]. This allows us to reduce the sintering temperature in the system, which in turn reduces the risk of sublimation of the sintered components, including the radioactive ones. Application of SPS-RS for fabrication of ceramics suitable for radionuclide immobilization is limited to a few reports studying chabazite [32], apatite [33], zirconate [34], zirconolite [35,36], scheelite [37], and feldspar [38]. SPS-RS fabrication of molybdate-based ceramics for radionuclide immobilization was not conducted before, to the best of our knowledge.

In this paper, the SPS-RS method is presented as a cumulative system in which simultaneous synthesis of the material and its ceramization takes place. In terms of synthesis, this method can be compared only with the method of solid-phase reaction followed by pressing and sintering [14]. The advantage of SPS technology becomes evident due to the shorter production cycle and one-stage production, and simultaneously applied pressure allows us to obtain ceramics with high parameters of mechanical strength.

It is important to note that many ceramics will be needed to immobilize large amounts of radioactive strontium. The final calculations of such ceramics are complex, as each

specific case of radionuclide handling presents individual challenges. Industrial versions of SPS systems, such as the JXP series [39], can provide for the production of large quantities of ceramics. Such a system allows the production of samples with a diameter of up to 300 mm, and it can also be designed as a conveyor system. Such a system can significantly reduce the production time, which is especially important when dealing with radioactive waste.

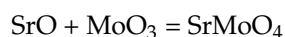
Thus, this paper aims to investigate the solid-phase synthesis of SrMoO₄ ceramics with a powellite structure via the SPS-RS fabrication pathway. This approach allows us to form solid-state matrixes with high exploitation characteristics, including hydrolytic stability, and which are suitable for the safe immobilization of Sr radionuclides.

2. Experimental

2.1. Reagents

The main precursors for the sample synthesis, namely, strontium oxide (SrO, 99.9%) and molybdenum oxide (MoO₃, 99.9%), were purchased from Sigma Aldrich (St. Louis, MI, USA) and were used as received.

SrMoO₄ ceramics was formed according to the following equation:



2.2. Reactive Mixture Preparation

The reactive mixture was prepared via ball milling of SrO (4.20 g) and MoO₃ (5.82 g) oxides on a Tencan XQM-0.4A planetary mill at 870 rpm for 7 cycles of 15 min each, with a 15 min break in between.

2.3. SPS-RS Fabrication of SrMoO₄ Ceramics

SrMoO₄ ceramics were fabricated using the SPS-RS approach on an SPS-515S sintering setup ("Dr. Sinter·LABTM", Kyoto, Japan), according to the following scheme. The reactive mixture was placed into the graphite die (internal diameter 15.5 mm), prepressed at 20.7 MPa, transferred into a vacuum chamber (10⁻⁵ atm), and sintered. Heating was provided by unipolar low-voltage pulse current in on/off regime with pulse/pause periodicity 12/2 and duration 39.6/6.6 ms. SPS temperature was controlled via an optical pyrometer (low limit of detection was 650 °C), focused on a 5.5 mm deep gap in the middle of the outer die wall. To prevent the powder from baking onto the die inner walls and plunges as well as to ease the ceramic extraction, we used 200 µm graphite foil. The die was wrapped in a thermal-insulating fabric to reduce the heat loss. Diameter and height of the obtained matrixes in the form of a cylinder were 15.3 mm and 4–10 mm (depending on the sintering temperature), respectively.

Final sintering temperature spanned 800–1200 °C, and heating rate was changed in stages: 300 °C/min below 650 °C, and 50 °C/min above 650 °C, when the working range of the pyrometer was reached. Holding time at final temperature was 5 min, then samples were cooled down to room temperature for 30 min. Mechanical load during the whole process was kept constant at 24.5 MPa.

2.4. Ceramics Preparation Prior to Characterization

To remove graphite foil from the ceramic surface, coarse polishing was conducted on the first stage using silicon carbide sandpaper with the grain sizes US CAMI 80, 120, and 240 (Allied High Tech Products, Inc., Compton, CA, USA). Then, the fine polishing was performed using silicon carbide sandpaper with grain sizes US CAMI 400, 600, 800, and 1200, followed by polishing with colloidal diamond suspension with 9, 3, and 1 µm and 0.04 µm sized particles (Allied High Tech Products, Inc., Compton, CA, USA) on a PRESI MECATECH 234 polishing machine (Eybens, France).

2.5. Characterization Methods

Particle size distribution was determined on a particle size analyzer G3-ID manufactured by Malvern Instruments Ltd. (Malvern, UK). Scanning electron microscopy (SEM) was performed on a CrossBeam 1540 XB manufactured by Carl Zeiss (Jena, Germany), equipped with the add-on for energy-dispersive spectral analysis (EDX) by Bruker (Mannheim, Germany). XRD was carried out on a D8 Advance Bruker AXS (Mannheim, Germany) diffractometer. The grain size distributions and the average grain sizes were calculated by the linear intercept method using scanning electron microscopy (SEM) images [40]. At least 300 grains for each sample were analyzed for each measurement. Vickers microhardness (HV) was determined at 0.2 N load on the microhardness tester HMV-G-FA-D manufactured by Shimadzu (Kyoto, Japan). Compressive strength (σ_{cs}) was evaluated on the tensile machine Autograph AG-X plus 100 kN manufactured by Shimadzu (Kyoto, Japan). Experimental density (ED) was measured by hydrostatic weighing on the balance Adventurer™ manufactured by OHAUS Corporation (Parsippany, NJ, USA). Relative density (RD) was found as a ratio of the experimental density (ED) measured via hydrostatic weighing to the theoretical density (TD).

Raman spectroscopy was carried out with an automated confocal micro-Raman setup (NTEGRA Spectra II, NT-MDT) equipped with a grating type spectrometer (M522, Solar Laser Systems) and a CCD-camera (i-Dus, Andor Technologies, Belfast, UK). Raman scattered from the isolated hemispherical NPs was excited by unpolarized fiber-coupled CW laser radiation (633 nm pump wavelengths) focused on the sample surface with a dry microscope objective (NA = 0.7; 100x Mitutoyo Apo).

Hydrolytic stability of matrixes was estimated based on desalination rate of strontium under long-term contact (30 days) with distilled water (pH 6.8) at room temperature (25 °C) in static conditions according to a well-known Russian Government Standard (GOST R 52126-2003), closely related to the ANSI/ANS—American National Standards Institute/American Nuclear Society 2019 (ANSI/ANS 16.1), which was updated according to the older procedure recommended by IAEA (ISO 6961:1982). Strontium ion concentrations were determined by inductively coupled plasma atomic emission spectrometry (ICP-MS) on an iCAP 7600 Duo spectrometer (Thermo Scientific, Waltham, MA, USA, 2013).

3. Results and Discussion

Fabrication of mineral-like ceramics with a powellite structure was based on the initiation of the “in situ” interaction between the oxides within the green body in the moment of SPS consolidation according to the following equation:



According to particle size analysis (Figure 1a), the initial oxide blend is characterized by a wide bimodal fractional distribution in the range 0.1–10 μm , with mean sizes 0.2 and 2 μm corresponding to the two modes. Particle size data are confirmed by SEM images, showing that the reactive powder blend possesses polydisperse size composition (Figure 1b), with the small-sized fraction consisting of needle-shaped particles. Large particles are relatively homogeneously distributed within the small particle fraction.

Based on the temporal and thermal evolution of SPS consolidation (Figure 2a,b), it was found that sintering proceeds in two stages regardless of the final sintering temperature. The first stage encompasses mechanical densification of powder particles and their partial deformation, rearrangement, and packing under constantly applied pressure. The second densification stage at 580–650 °C is a result of chemical interaction yielding the SrMoO_4 phase and thermal consolidation of particles forming a dense compact. This stage manifests in the active atomic diffusion along the interparticle contacts, viscous flow, and particle plastic deformation, leading to overall material compaction. The sample sintered at 1200 °C observed a third densification stage, likely caused by the sublimation of molybdenum oxide at 1155 °C in accordance with references [41].

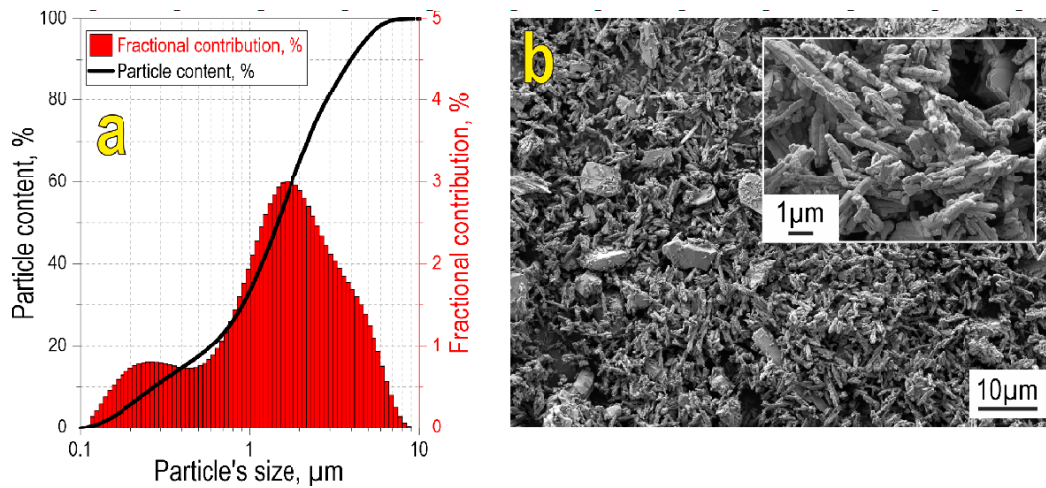


Figure 1. Particle size distribution (a) and SEM image (b) of the initial reactive powder blend. The inset in (b) shows the SEM image of the initial blend at higher magnification.

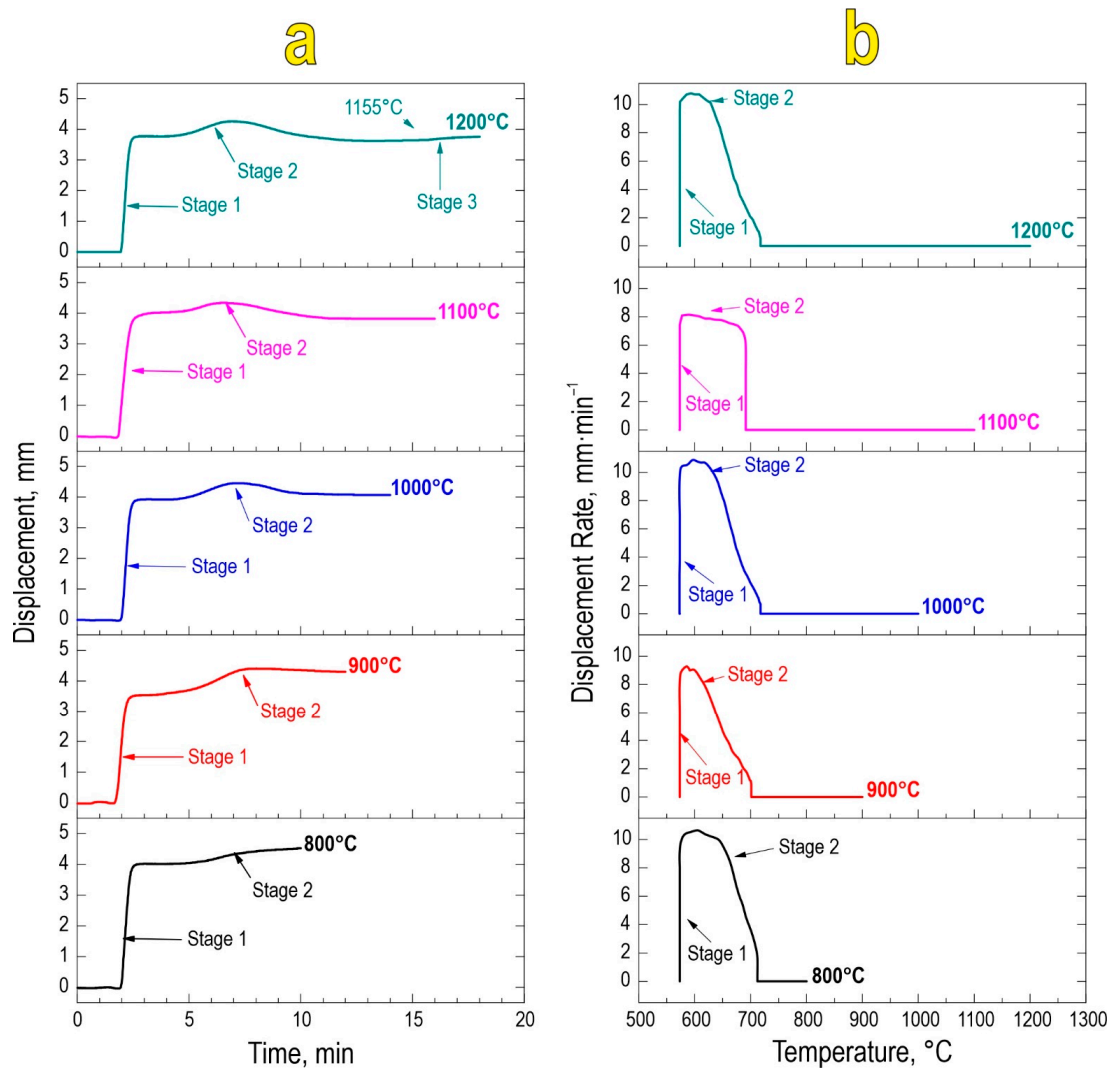


Figure 2. Consolidation dynamics of the reactive powder blend during SPS-RS, expressed as densification rate vs. time (a) and temperature (b).

According to XRD (Figure 3), the reactive interaction within the oxide blend leading to SrMoO_4 formation under SPS proceeds successfully at all studied temperatures in the range 800–1200 °C. The intensity of diffraction maxima increases with the temperature. However, at 1200 °C, SrMoO_4 starts to decompose back into oxides due to the sublimation of MoO_3 occurring at 1155 °C, according to the previously reported data [41]. Pronounced decomposition can be a result of the vacuum employed during sintering, which promotes the removal of sublimated molybdenum oxide and shifts the equilibrium towards the reverse reaction. The presented data indicate the isomorphism of the CaMoO_4 - SrMoO_4 structure and the possibility of Ca^{2+} substitution by Sr^{2+} . The theoretical possibility of isomorphous substitution is proved by Goldschmidt's law, which agrees on the following points:

1. Ion sizes should differ by no more than 10–15%. The ionic radius of Ca^{2+} is 1.04 Å and the ionic radius of Sr^{2+} is 1.2 Å, resulting in a difference of 14%.
2. The difference in electronegativity is less than 0.4. The electronegativity of Ca^{2+} is 1.00 and that of Sr^{2+} is 0.95, resulting in a difference of 0.05.

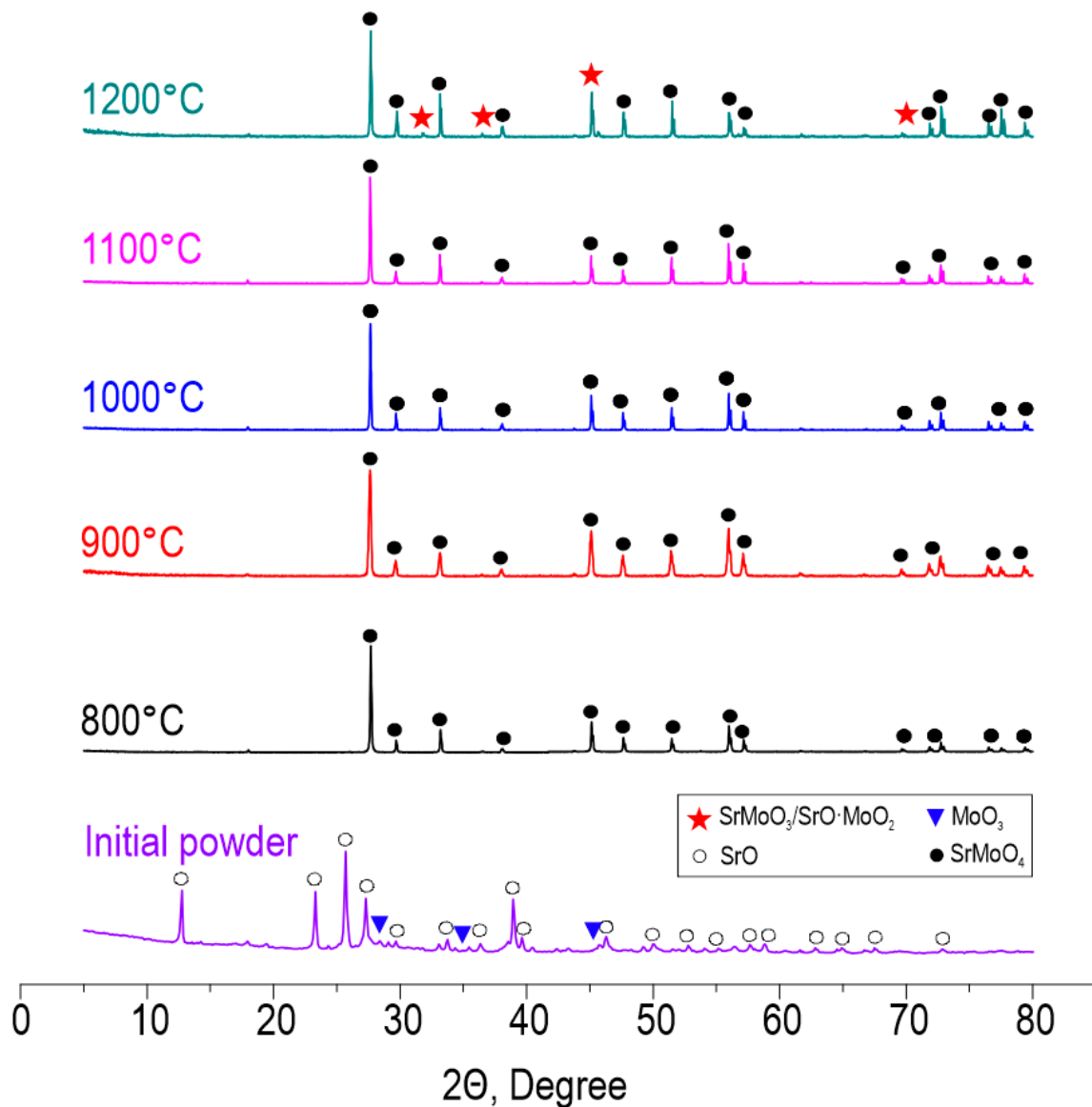


Figure 3. XRD patterns of the initial reactive powder blend and ceramic samples derived thereof at various SPS-RS temperatures.

As can be seen, the conditions of isomorphism are fulfilled.

The structure of strontium molybdate has also been investigated by Raman spectroscopy (Figure 4). Raman spectra of molybdates include internal and external vibrational modes. Raman spectra of sintered SrMoO₄ ceramic sample powders with ten observed and labeled vibrational modes are shown in Figure 4. The internal modes ν_1 , ν_2 , ν_3 , and ν_4 are at 328, 365/366, 382, 796, 844, and 887 cm⁻¹. The external modes are observed around 93–139 cm⁻¹ and the free-spinning modes are observed at 182/179 cm⁻¹, which is in agreement with the literature data.

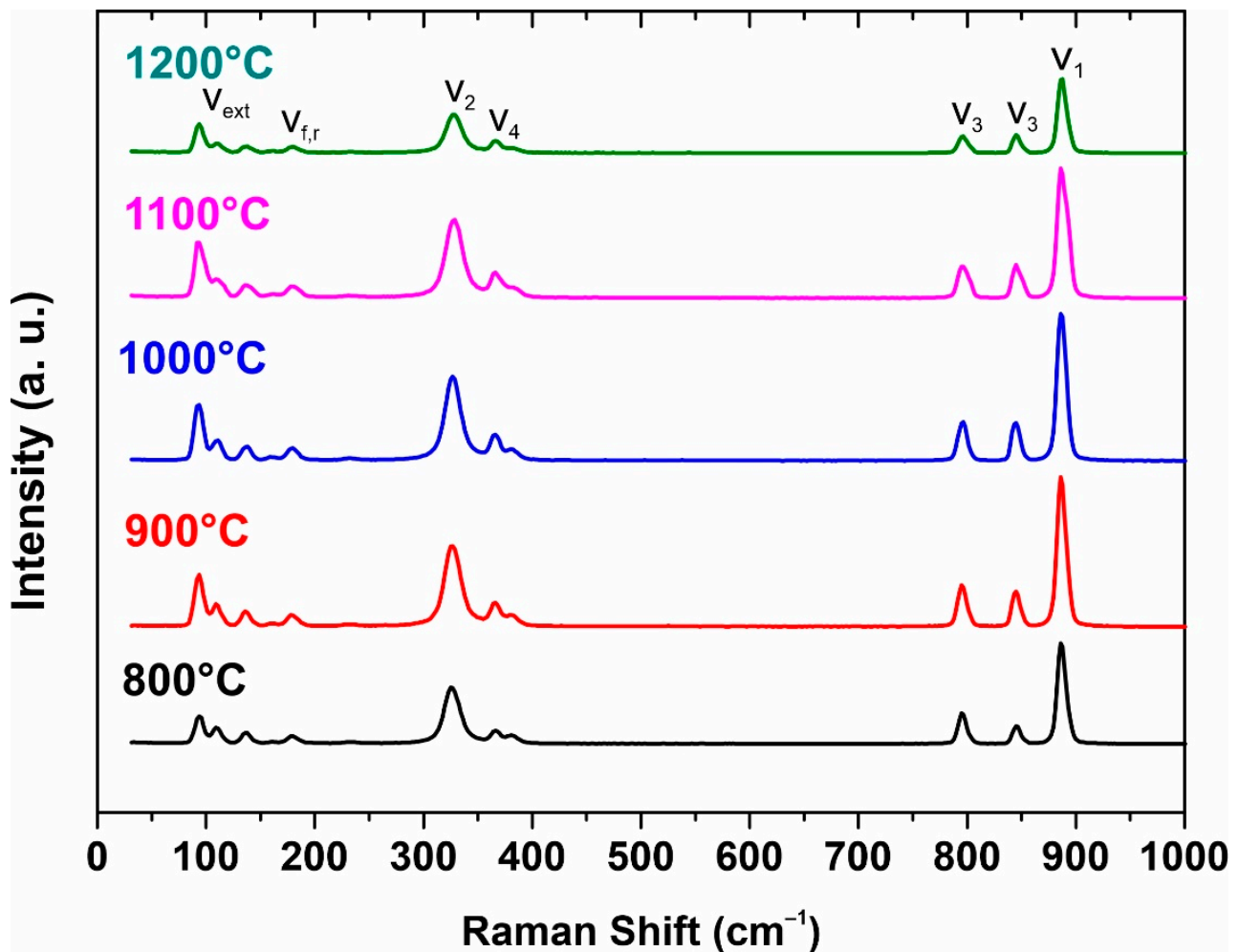


Figure 4. Raman spectra from initial powder to 1200 °C sample.

SEM images reveal that the morphology of the powder particles of the starting reactive mixture significantly changes under SPS (Figure 5). The structure of the formed ceramics is presented by well-faceted grains. An increase in the reactive sintering temperature induces dramatic grain growth. Samples sintered at 800–1200 °C are characterized by the presence of macroporous formations. On the other hand, porosity diminishes at higher sintering temperatures, owing to the grain growth indicated above. The surface of the ceramics sintered at 1100–1200 °C approaches a monolith.

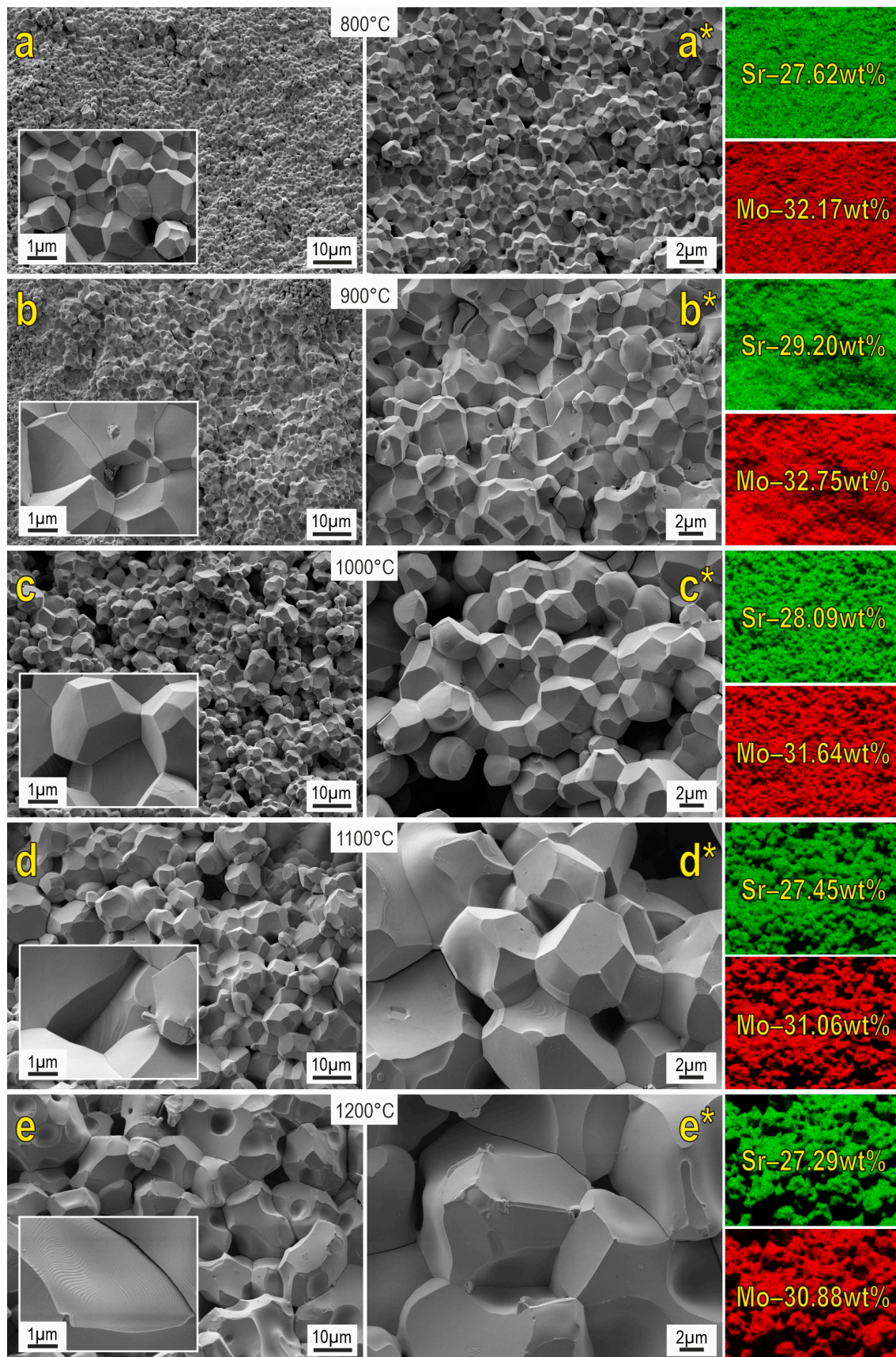


Figure 5. SEM images and EDX analysis of SrMoO₄ ceramics sintered at various SPS-RS temperatures.

EDX data revealed that the distribution of the main elements on the shears of the analyzed surface is uniform. When comparing the obtained data with the literature sources [10,12,14], the similar morphology of particles as well as their dimensionality can be observed.

The analysis of the morphology indicates that the samples obtained at sintering temperatures of 800–900 °C are characterized by a narrow grain size distribution with a predominance of grains of the smallest fractions (up to 2 µm) (Figure 6). The maximum size does not exceed 10 µm. The average grain sizes (d_{AV}) for 800 °C and 900 °C samples are 2.6 and 2.9 µm, respectively. Starting at 1000 °C, a lognormal grain size distribution begins to form, and each subsequent 100 °C increase in SPS temperature leads to a twofold increase in average grain size. The grain distribution of the sample obtained at 1100 °C is well described by the lognormal function; the coefficient of determination is $R^2 = 0.968$ and $d_{AV} = 9.7$ µm. The broadening of the distribution at 1200 °C ($R^2 = 0.895$) indicates recrystallization processes in the system due to phase decomposition into the initial oxides. Maximum grain size reaches 54 µm.

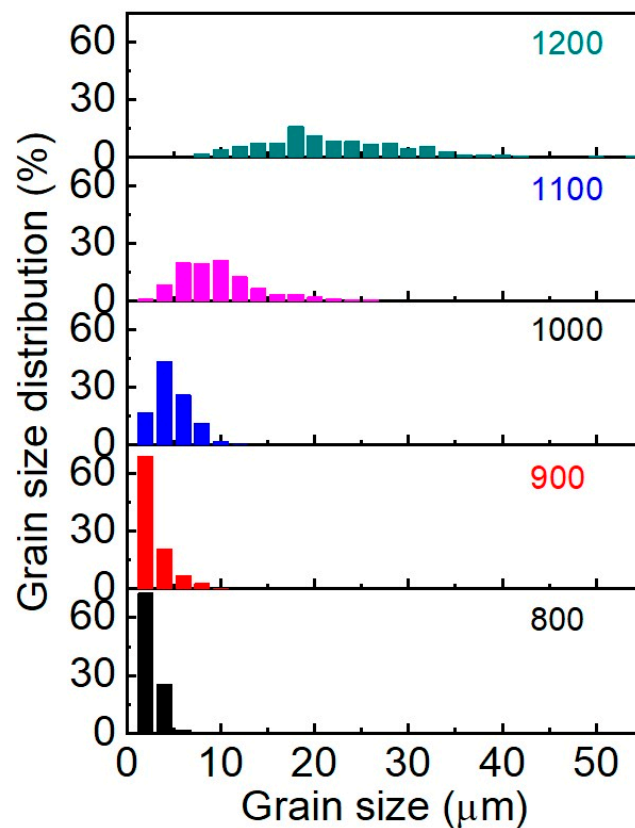


Figure 6. Grain size distribution of SrMoO₄ SPS samples at 800–1200 °C.

The physicochemical characteristics of the ceramics, namely, relative density (84.0–96.3%), compressive strength (54–331 MPa), and Vickers microhardness (157–295 HV), increase with the sintering temperature (Figure 7a). A scatter plot of Vickers microhardness allows us to assess the mechanical microheterogeneity of the material (Figure 7b). According to the data, we found that each sample observed some variation in microhardness values caused by anisotropy of the studied characteristics in local parts of the sample. The sample sintered at 1100 °C observed increased heterogeneity in terms of microhardness, which is likely caused by molybdenum oxide sublimation. However, the sample sintered at 1200 °C exhibited much higher values of microhardness, probably due to the formation of separate phases of SrO and MoO₃, which act as alloying agents strengthening the ceramic particles. Also, the effect of consolidation at 1200 °C is maximal compared to lower temperatures, yielding ceramics of higher mechanical strength.

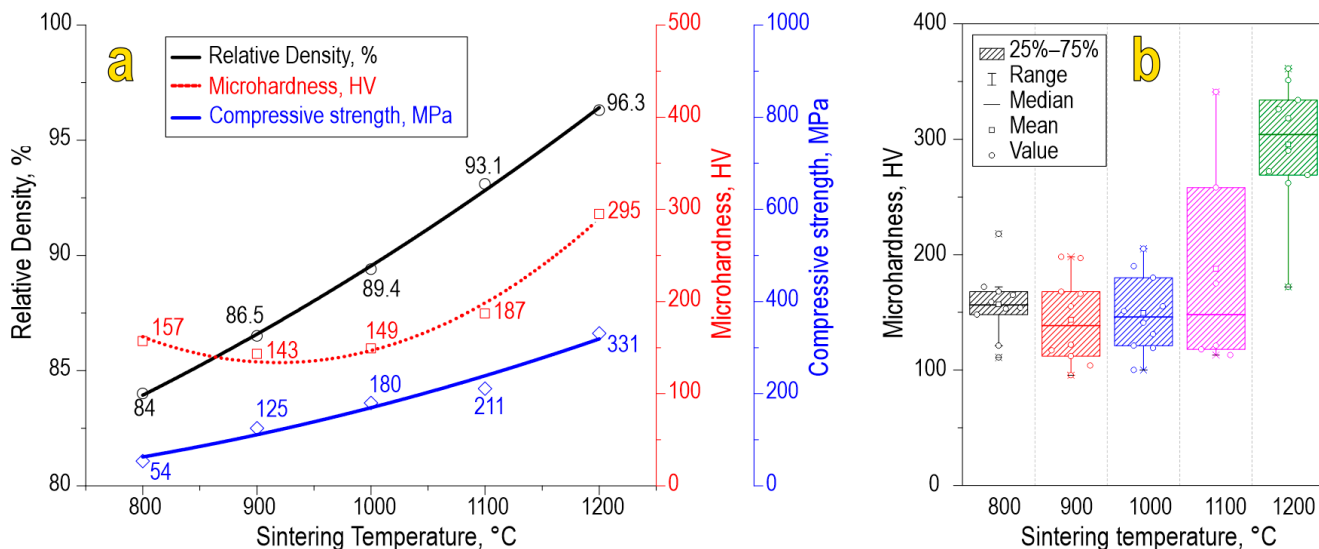


Figure 7. Physicochemical characteristics (a) and scatter plot of Vickers microhardness (b) for SrMoO₄ ceramics sintered at various SPS-RS temperatures.

As-prepared SrMoO₄ ceramics were subjected to hydrolytic stability tests in terms of strontium discharge. The strontium leaching rate for all samples was as low as 10⁻⁶ g/cm²·day (Figure 8). The ceramic sample obtained at 1200 °C was characterized by a higher strontium leaching rate, even compared to the sample sintered at 800 °C. This effect is caused by the change in phase composition due to molybdenum oxide sublimation, proven by XRD above (Figure 3). It is noteworthy that all leaching rate values meet the requirements of ISO 6961:1982 and GOST R 50926-96, indicating the high hydrolytic stability of ceramics.

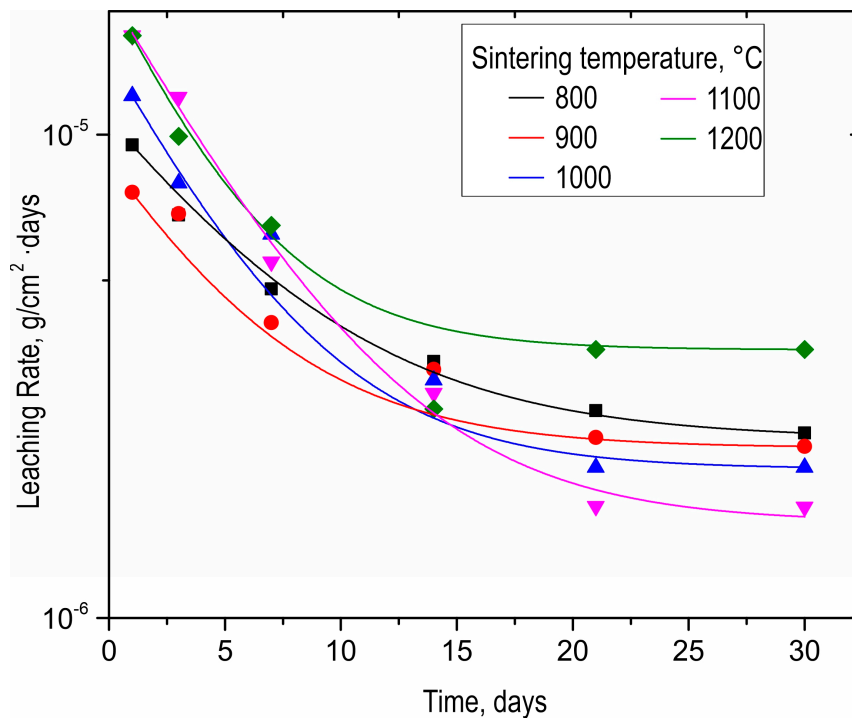


Figure 8. Leaching rate of strontium from SrMoO₄ ceramics sintered at various SPS-RS temperatures during long-term (30 days) contact with distilled water.

4. Conclusions

We realized the spark plasma sintering–reactive sintering strategy to fabricate SrMoO₄ mineral-like ceramics adopting a powellite structure, which is a promising candidate for the immobilization of the high-energy ⁹⁰Sr isotope. “In situ” consolidation dynamics of a SrO/MoO₃ reactive powder blend were studied for the case of SPS. Dilatometry, XRD, SEM, and EDX methods were used to identify the main stages of reactive powder blend densification related to mechanical compaction and solid-state processes of sintering under thermal heating. Phase formation and structural and compositional changes of the formed ceramics were studied. The decomposition of the SrMoO₄ phase into starting oxides above 1100 °C was revealed. Sintering was found to cause active grain growth, leading to the formation of a nonporous polydisperse ceramic structure. Higher sintering temperatures increase the relative porosity (84.0–96.3%), compressive strength (54–331 MPa), and Vickers microhardness (157–295 HV), with the sample obtained at 1200 °C attaining the best properties so far. All fabricated ceramics demonstrated low leaching rates of 10^{−6} g/cm²·day, indicating high hydrolytic stability that meets the requirements of GOST R 50926-96 and ISO 6961:1982 imposed on highly radioactive solid wastes.

Author Contributions: Conceptualization, O.O.S., I.Y.B. and E.A.G.; Methodology, A.A.B., O.O.S., S.A.A., E.S.K. and E.A.G.; Software, I.Y.B.; Validation, I.Y.B. and S.A.A.; Formal analysis, A.N.F.; Investigation, A.A.B., A.S.P., A.P., N.B.K. and Y.S.; Data curation, A.A.B., A.S.P., A.A.V., A.N.F. and E.S.K.; Writing—original draft, O.O.S., E.K.P. and I.G.T.; Writing—review & editing, O.O.S., E.K.P. and I.G.T.; Project administration, E.K.P.; Funding acquisition, E.K.P. All authors have read and agreed to the published version of the manuscript.

Funding: This study was financially supported within the State Assignment of the Ministry of Science and Higher Education of the Russian Federation, topic No. FZNS-2023-0003. The equipment of the Joint Center for Collective Use, the interdisciplinary center in the field of nanotechnology and new functional materials of the FEFU, was used in this work (Vladivostok, Russia).

Institutional Review Board Statement: Not applicable for studies not involving humans or animals.

Data Availability Statement: There are no databases or archives. All obtained results are displayed in the publication.

Conflicts of Interest: The authors declare no conflict of interest.

References

1. Potanina, E.A.; Orlova, A.I.; Mikhailov, D.A.; Nokhrin, A.V.; Chuvil'deev, V.N.; Boldin, M.S.; Sakharov, N.V.; Lantsev; Tokarev, M.G.; Murashov, A.A. Spark Plasma Sintering of Fine-Grained SrWO₄ and NaNd(WO₄)₂ Tungstates Ceramics with the Scheelite Structure for Nuclear Waste Immobilization. *J. Alloys Compd.* **2019**, *774*, 182–190. [[CrossRef](#)]
2. Brinkman, K.; Fox, K.; Marra, J.; Reppert, J.; Crum, J.; Tang, M. Single Phase Melt Processed Powellite (Ba,Ca)MoO₄ for the Immobilization of Mo-Rich Nuclear Waste. *J. Alloys Compd.* **2013**, *551*, 136–142. [[CrossRef](#)]
3. Peterson, J.A.; Crum, J.V.; Riley, B.J.; Asmussen, R.M.; Neeway, J.J. Synthesis and Characterization of Oxyapatite [Ca₂Nd₈(SiO₄)₆O₂] and Mixed-Alkaline-Earth Powellite [(Ca,Sr,Ba)MoO₄] for a Glass-Ceramic Waste Form. *J. Nucl. Mater.* **2018**, *510*, 623–634. [[CrossRef](#)]
4. Patel, K.B.; Boizot, B.; Facq, S.P.; Lampronti, G.I.; Peugeot, S.; Schuller, S.; Farnan, I. β-Irradiation Effects on the Formation and Stability of CaMoO₄ in a Soda Lime Borosilicate Glass Ceramic for Nuclear Waste Storage. *Inorg. Chem.* **2017**, *56*, 1558–1573. [[CrossRef](#)]
5. Maltsev, D.A.; Lomachuk, Y.V.; Shakhova, V.M.; Mosyagin, N.S.; Skripnikov, L.V.; Titov, A.V. Compound-Tunable Embedding Potential Method and Its Application to Calcium Niobate Crystal CaNb₂O₆ with Point Defects Containing Tantalum and Uranium. *Phys. Rev. B* **2021**, *103*, 205105. [[CrossRef](#)]
6. Spano, T.L.; Olds, T.A.; Hall, S.M.; Van Gosen, B.S.; Kampf, A.R.; Burns, P.C.; Marty, J. Finchite, Sr(UO₂)₂(V₂O₈)·5H₂O, a New Uranyl Sorovanadate with the Francevillite Anion Topology. *Am. Mineral.* **2023**, *108*, 383–388. [[CrossRef](#)]
7. Banerjee, C.; Dudwadkar, N.; Tripathi, S.C.; Gandhi, P.M.; Grover, V.; Kaushik, C.P.; Tyagi, A.K. Nano-Cerium Vanadate: A Novel Inorganic Ion Exchanger for Removal of Americium and Uranium from Simulated Aqueous Nuclear Waste. *J. Hazard. Mater.* **2014**, *280*, 63–70. [[CrossRef](#)]
8. Çiftçiyürek, E.; Sabolsky, K.; Sabolsky, E.M. Molybdenum and Tungsten Oxide Based Gas Sensors for High Temperature Detection of Environmentally Hazardous Sulfur Species. *Sens. Actuators B Chem.* **2016**, *237*, 262–274. [[CrossRef](#)]

9. Liu, F.; Wang, J.; Jiang, L.; You, R.; Wang, Q.; Wang, C.; Lin, Z.; Yang, Z.; He, J.; Liu, A.; et al. Compact and Planar Type Rapid Response Ppb-Level SO₂ Sensor Based on Stabilized Zirconia and SrMoO₄ Sensing Electrode. *Sens. Actuators B Chem.* **2020**, *307*, 127655. [[CrossRef](#)]
10. Tian, X.; Guo, L.; Wen, J.; Zhu, L.; Ji, C.; Huang, Z.; Qiu, H.; Luo, F.; Liu, X.; Li, J.; et al. Anti-Thermal Quenching Behavior of Sm³⁺ Doped SrMoO₄ Phosphor for New Application in Temperature Sensing. *J. Alloys Compd.* **2023**, *959*, 170574. [[CrossRef](#)]
11. De Azevedo Marques, A.P.; Umisedo, N.K.; Costa, J.A.; Yoshimura, E.M.; Okuno, E.; Künzel, R. The Role of Capping Agents on the Trapping Levels Structure and Luminescent Emission of SrMoO₄ Phosphors. *J. Lumin.* **2023**, *257*, 119662. [[CrossRef](#)]
12. Thirimal, C.; Ramarao, S.D.; Rao, L.S.; Murthy, V.R.K. Study of Structural, Dielectric and AC Conductivity Properties of SrMoO₄. *Mater. Res. Bull.* **2022**, *146*, 111618. [[CrossRef](#)]
13. Pankratova, V.; Dunaeva, E.E.; Voronina, I.S.; Kozlova, A.P.; Shendrik, R.; Pankratov, V. Luminescence Properties and Time-Resolved Spectroscopy of Rare-Earth Doped SrMoO₄ Single Crystals. *Opt. Mater. X* **2022**, *15*, 100169. [[CrossRef](#)]
14. Mikhaylovskaya, Z.A.; Buyanova, E.S.; Malkin, A.I.; Korotkov, A.N.; Knyazev, N.S.; Petrova, S.A. Morphological and Microwave Dielectric Properties of Bi:SrMoO₄ Ceramic. *J. Solid State Chem.* **2022**, *316*, 123555. [[CrossRef](#)]
15. Künzel, R.; Umisedo, N.K.; Okuno, E.; Yoshimura, E.M.; Marques, A.P.d.A. Effects of Microwave-Assisted Hydrothermal Treatment and Beta Particles Irradiation on the Thermoluminescence and Optically Stimulated Luminescence of SrMoO₄ Powders. *Ceram. Int.* **2020**, *46*, 15018–15026. [[CrossRef](#)]
16. Künzel, R.; Feldhaus, C.M.S.; Suzuki, Y.O.F.; Ferreira, F.F.; de Paula, V.G.; Courrol, L.C.; Umisedo, N.K.; Yoshimura, E.M.; Okuno, E.; de Azevedo Marques, A.P. Photoluminescence and Magnetic Properties of SrMoO₄ Phosphors Submitted to Thermal Treatment and Electron Irradiation. *J. Magn. Magn. Mater.* **2022**, *562*, 169761. [[CrossRef](#)]
17. Chavan, A.B.; Gawande, A.B.; Gaikwad, V.B.; Jain, G.H.; Deore, M.K. Hydrothermal Synthesis and Luminescence Properties of Dy³⁺ Doped SrMoO₄ Nano-Phosphor. *J. Lumin.* **2021**, *234*, 117996. [[CrossRef](#)]
18. Jung, J. Luminescent Color-Adjustable Europium and Terbium Co-Doped Strontium Molybdate Phosphors Synthesized at Room Temperature Applied to Flexible Composite for LED Filter. *Crystals* **2022**, *12*, 552. [[CrossRef](#)]
19. Mikhailik, V.B.; Elyashevskiy, Y.; Kraus, H.; Kim, H.J.; Kapustianyk, V.; Panasyuk, M. Temperature Dependence of Scintillation Properties of SrMoO₄. *Nucl. Instrum. Methods Phys. Res. Sect. A Accel. Spectrom. Detect. Assoc. Equip.* **2015**, *792*, 1–5. [[CrossRef](#)]
20. Meng, C.; Li, W.; Ren, C.; Zhao, J. Structure and Chemical Durability Studies of Powellite Ceramics Ca_{1-x}Li_{x/2}Gd_{x/2}MoO₄ (0 ≤ x ≤ 1) for Radioactive Waste Storage. *J. Mater. Sci.* **2020**, *55*, 2741–2749. [[CrossRef](#)]
21. Neeway, J.J.; Asmussen, R.M.; McElroy, E.M.; Peterson, J.A.; Riley, B.J.; Crum, J.V. Kinetics of Oxyapatite [Ca₂Nd₈(SiO₄)₆O₂] and Powellite [(Ca,Sr,Ba)MoO₄] Dissolution in Glass-Ceramic Nuclear Waste Forms in Acidic, Neutral, and Alkaline Conditions. *J. Nucl. Mater.* **2019**, *515*, 227–237. [[CrossRef](#)]
22. Karaeva, M.E.; Savinykh, D.O.; Orlova, A.I.; Khainakov, S.A.; Nokhrin, A.V.; Boldin, M.S.; Garcia-Granda, S.; Murashov, A.A.; Chuvil'deev, V.N.; Yunin, P.A.; et al. (Na, Zr) and (Ca, Zr) Phosphate-Molybdates and Phosphate-Tungstates: I-Synthesis, Sintering and Characterization. *Materials* **2023**, *16*, 990. [[CrossRef](#)] [[PubMed](#)]
23. Ranganatha, C.L.; Loksha, H.S.; Nagabhushana, K.R.; Palakshamurthy, B.S. Studies on Luminescence Properties of Self-Activated SrMoO₄ Phosphor: Kinetic Analysis. *J. Alloys Compd.* **2023**, *962*, 171061. [[CrossRef](#)]
24. Hu, Z.Y.; Zhang, Z.H.; Cheng, X.W.; Wang, F.C.; Zhang, Y.F.; Li, S.L. A Review of Multi-Physical Fields Induced Phenomena and Effects in Spark Plasma Sintering: Fundamentals and Applications. *Mater. Des.* **2020**, *191*, 108662. [[CrossRef](#)]
25. Orlova, A.I.; Ojovan, M.I. Ceramic Mineral Waste-Forms for Nuclear Waste Immobilization. *Materials* **2019**, *12*, 2638. [[CrossRef](#)]
26. Papynov, E.K.; Shichalin, O.O.; Belov, A.A.; Buravlev, I.Y.; Portnyagin, A.S.; Azon, S.A.; Shlyk, D.K.; Buravleva, A.A.; Parot'kina, Y.A.; Nepomnyushchaya, V.A.; et al. Synthesis of Mineral-Like SrWO₄ Ceramics with the Scheelite Structure and a Radioisotope Product Based on It. *Russ. J. Inorg. Chem.* **2021**, *66*, 1434–1446. [[CrossRef](#)]
27. Orlova, A.I. Crystalline Phosphates for HLW Immobilization—Composition, Structure, Properties and Production of Ceramics. Spark Plasma Sintering as a Promising Sintering Technology. *J. Nucl. Mater.* **2022**, *559*, 153407. [[CrossRef](#)]
28. Papynov, E.K.; Shichalin, O.O.; Mayorov, V.Y.; Kuryavyi, V.G.; Kaidalova, T.A. SPS Technique for Ionizing Radiation Source Fabrication Based on Dense Cesium-Containing Core. *J. Hazard. Mater.* **2019**, *369*, 25–30. [[CrossRef](#)]
29. Papynov, E.K.; Shichalin, O.O.; Belov, A.A.; Buravlev, I.Y.; Portnyagin, A.S.; Kozlov, A.G.; Gridasova, E.A.; Tananaev, I.G.; Sergienko, V.I. Ionizing Radiation Source-Open Type Fabrication Using Additive Technology and Spark Plasma Sintering. *Ceram. Int.* **2023**, *49*, 3083–3087. [[CrossRef](#)]
30. Dudina, D.V.; Mukherjee, A.K. Reactive Spark Plasma Sintering: Successes and Challenges of Nanomaterial Synthesis. *J. Nanomater.* **2013**, *2013*, 625218. [[CrossRef](#)]
31. Mukasyan, A.S.; Rogachev, A.S.; Moskovskikh, D.O.; Yermekova, Z.S. Reactive Spark Plasma Sintering of Exothermic Systems: A Critical Review. *Ceram. Int.* **2022**, *48*, 2988–2998. [[CrossRef](#)]
32. Harnett, L.C.; Gardner, L.J.; Sun, S.K.; Mann, C.; Hyatt, N.C. Reactive Spark Plasma Sintering of Cs-Exchanged Chabazite: Characterisation and Durability Assessment for Fukushima Daiichi NPP Clean-Up. *J. Nucl. Sci. Technol.* **2019**, *56*, 891–901. [[CrossRef](#)]
33. Le Gallet, S.; Campayo, L.; Courtois, E.; Hoffmann, S.; Grin, Y.; Bernard, F.; Bart, F. Spark Plasma Sintering of Iodine-Bearing Apatite. *J. Nucl. Mater.* **2010**, *400*, 251–256. [[CrossRef](#)]
34. Wang, L.; Shu, X.; Lu, X.; Wu, Y.; Ding, Y.; Zhang, S. Rapid Synthesis of High Densified Single Phase Ceramic Gd₂Zr₂O₇ by Spark Plasma Sintering. *Mater. Lett.* **2017**, *196*, 403–405. [[CrossRef](#)]

35. Sun, S.K.; Stennett, M.C.; Corkhill, C.L.; Hyatt, N.C. Reactive Spark Plasma Synthesis of $\text{CaZrTi}_2\text{O}_7$ Zirconolite Ceramics for Plutonium Disposition. *J. Nucl. Mater.* **2018**, *500*, 11–14. [[CrossRef](#)]
36. Blackburn, L.R.; Sun, S.; Lawson, S.M.; Gardner, L.J.; Ding, H.; Corkhill, C.L.; Maddrell, E.R.; Stennett, M.C.; Hyatt, N.C. Synthesis and Characterisation of $\text{Ca}_{1-x}\text{Ce}_x\text{ZrTi}_{2-2x}\text{Cr}_{2x}\text{O}_7$: Analogue Zirconolite Wasteform for the Immobilisation of Stockpiled UK Plutonium. *J. Eur. Ceram. Soc.* **2020**, *40*, 5909–5919. [[CrossRef](#)]
37. Papynov, E.K.; Shichalin, O.O.; Buravlev, I.Y.; Belov, A.A.; Portnyagin, A.S.; Fedorets, A.N.; Azarova, Y.A.; Tananaev, I.G.; Sergienko, V.I. Spark Plasma Sintering-Reactive Synthesis of SrWO_4 Ceramic Matrices for ^{90}Sr Immobilization. *Vacuum* **2020**, *180*, 109628. [[CrossRef](#)]
38. Papynov, E.K.; Belov, A.A.; Shichalin, O.O.; Buravlev, I.Y.; Azon, S.A.; Golub, A.V.; Gerasimenko, A.V.; Parotkina, Y.; Zavjalov, A.P.; Tananaev, I.G.; et al. $\text{SrAl}_2\text{Si}_2\text{O}_8$ Ceramic Matrices for ^{90}Sr Immobilization Obtained via Spark Plasma Sintering-Reactive Synthesis. *Nucl. Eng. Technol.* **2021**, *53*, 2289–2294. [[CrossRef](#)]
39. Tokita, M. Recent Advanced Spark Plasma Sintering (SPS) Technology, Systems and Applications in Japan. In Proceedings of the 1st Russia-Japan SPS Workshop, Moscow, Russia, 20–22 May 2013.
40. Wurst, J.C.; Nelson, J.A. Lineal Intercept Technique for Measuring Grain Size in Two-Phase Polycrystalline Ceramics. *J. Am. Ceram. Soc.* **1972**, *55*, 109. [[CrossRef](#)]
41. Wang, L.; Li, M.-C.; Xue, Z.-L.; Zhang, G.-H.; Huang, A. Sublimation Behavior of Industrial Grade Molybdenum Trioxide. *Trans. Indian Inst. Met.* **2021**, *74*, 1469–1477. [[CrossRef](#)]

Disclaimer/Publisher’s Note: The statements, opinions and data contained in all publications are solely those of the individual author(s) and contributor(s) and not of MDPI and/or the editor(s). MDPI and/or the editor(s) disclaim responsibility for any injury to people or property resulting from any ideas, methods, instructions or products referred to in the content.